

SUBMITTED VERSION

This is the pre-peer reviewed version of the following article:

Ruth E. Shaw, Christopher A. G. Kalnins, Nigel Antony Spooner, Carly Whittaker, Stephan Grimm, Kay Schuster, David Ottaway, Jillian Elizabeth Moffatt, Georgios Tsiminis, Heike Ebendorff-Heidepriem

Luminescence effects in reactive powder sintered silica glasses for radiation sensing
Journal of the American Ceramic Society, 2019; 102(1):222-238

which has been published in final form at <http://dx.doi.org/10.1111/jace.15918>. This article may be used for non-commercial purposes in accordance with Wiley Terms and Conditions for Use of Self-Archived Versions."

© 2018 The American Ceramic Society

PERMISSIONS

<https://authorservices.wiley.com/author-resources/Journal-Authors/licensing/self-archiving.html>

Submitted (preprint) Version

The submitted version of an article is the author's version that has not been peer-reviewed, nor had any value added to it by Wiley (such as formatting or copy editing).

The submitted version may be placed on:

- the author's personal website
- the author's company/institutional repository or archive
- not for profit subject-based preprint servers or repositories

Self-archiving of the submitted version is not subject to an embargo period. We recommend including an acknowledgement of acceptance for publication and, following the final publication, authors may wish to include the following notice on the first page:

"This is the pre-peer reviewed version of the following article: [FULL CITE], which has been published in final form at [Link to final article using the DOI]. This article may be used for non-commercial purposes in accordance with Wiley Terms and Conditions for Use of Self-Archived Versions."

The version posted may not be updated or replaced with the accepted version (except as provided below) or the final published version (the Version of Record).

There is no obligation upon authors to remove preprints posted to not for profit preprint servers prior to submission.

20 February, 2019

Title: Luminescence effects in reactive powder sintered silica glasses for radiation sensing

Authors: Ruth E Shaw^{i†}, Christopher A.G. Kalnins[‡], Nigel Antony Spooner^{†‡}, Carly Whittaker[‡], Stephan Grimm[#], Kay Schuster[#], David Ottaway[‡], Jillian Elizabeth Moffatt[‡], Georgios Tsiminis[‡] and Heike Ebendorff-Heidepriem[‡]

[‡] Institute for Photonics & Advanced Sensing and School of Physical Sciences, University of Adelaide, Adelaide, 5005, Australia

[‡] Australian Research Council Research Hub for Australian Copper-Uranium

[†] Defence Science & Technology Group, Edinburgh 5111, SA, Australia

[#] Leibniz Institute of Photonic Technology, Fibre Optics, Albert-Einstein-Str. 9, Jena, 07745, Germany

Abstract (should be < 200 words): Silica glasses doped with rare earth ions are potential materials for optical fibre radiation detection and dosimetry applications. High sensitivity to radiation requires fibres with large cores that can be reliably fabricated using glass made in a novel process from the reactive powder sintering of silica. The luminescence and dosimetric properties of a range of rare earth doped silica materials produced using this novel technique are reported here.

Radioluminescence and optically stimulated luminescence are the fundamental mechanisms enabling radiation detection in optical fibres. It was found that thermoluminescence, radioluminescence and optically stimulated luminescence are observed if the glass contains luminescent transitions in the detection wavelength range. Cerium and thulium doped silica glasses were found to be promising candidates for optical fiber dosimetry. Samples showed intense luminescence signals in response to both photo-stimulation and irradiation from alpha and beta sources. Optically stimulated luminescence results for cerium are three times larger than results for irradiated fluoride phosphate glasses previously tested for dosimetry use. Spectroscopic measurements indicate emission in the 300 to 500 nm region, suitable for detection with photomultiplier tubes.

ⁱ Corresponding author: ruth.shaw@adelaide.edu.au

1. Introduction

Previous research has shown intrinsic radiation-sensitive optical fibres to be a viable method of radiation detection, offering low-cost, low-power, real-time and near continuous monitoring in hard to access areas over extended detection lengths (1-3) making them ideal for radiation portal sensors and radiation dosimeters. The literature shows that most optical fiber dosimetry is done using scintillation, whilst reports of using optically stimulated luminescence (OSL) within an intrinsic optical fiber are limited (4). Previously, radiation detection using the OSL response from a fiber has been studied in fluoride phosphate glasses (4, 5). Silica offers a more physically robust and optically efficient alternative because silica has high mechanical strength (6), thermal resistance (7) and low optical loss (8) making silica very well suited for use as portal sensors requiring prompt sensing. Extrinsic doped sections attached to silica guiding fiber have been tested using OSL, however at this stage their extrinsic nature limits them to measuring single point locations (1, 9-12).

Single material large core unstructured fibers have the advantages of increased surface area and cross section which leads to a larger detection volume. They have also been shown to have improved OSL response (4, 5, 10). Photoluminescence transitions from rare earths can also enhance sensitivity in luminescence based detection techniques such as thermoluminescence, radioluminescence and OSL (13, 14). Additional elements such as aluminium, to improve the solubility of rare earths (15), and boron, to decrease the refractive index (15) and potentially cause oxidative fiber fabrication conditions, may also prove to be optimal glass structural components. Thus, an intrinsic fiber combining a single material unstructured large core containing aluminium and boron and doped with rare earth ions, potentially increases luminescence sensitivity to radiation, advantageous for OSL and scintillation measurements.

The Leibniz Institute of Photonic Technology and the Heraeus Group have pioneered a custom fabrication process of reactive powder sintering of silica (REPUSIL) (15-17). This technique allows single material large core fibers currently being made up to a diameter of 1.2 mm (15), that are unattainable using the Modified Chemical Vapour Deposit (MCVD) method. The MCVD doped core is

limited in diameter, generally up to 100 µm (15), and has been proven difficult in maintaining dopant concentrations, distribution and homogeneity (16). Melt quench techniques allow precise control of dopant concentration and homogeneous dopant distribution over larger volumes, but have higher loss (15). They are also less robust due to lower softening temperatures, compared to glass made using the REPUSIL technique. The REPUSIL method allows high purity homogeneous dopant addition to silica across large cores with high batch-to-batch reproducibility (17).

Here we report the first investigation of REPUSIL as a radiation sensor. We examine the sensitivity of radiation-induced luminescence attributed to rare earth dopants in bulk glass made using the newly available REPUSIL materials. This study is to determine if the REPUSIL technique can create a new class of materials for luminescence detection in large core intrinsic fibers. We made a range of rare earth doped samples containing rare earth ions susceptible to luminescent transitions; lanthanum (La), cerium (Ce), samarium (Sm), thulium (Tm) and ytterbium (Yb). Reference glasses containing non-luminescent dopants; boron (B) and aluminium (Al), were also made using the REPUSIL process. The optical and dosimetric properties of these rare earth doped and reference samples were characterised. Absorption and emission spectra were obtained to determine the most appropriate optical stimulation wavelength and signal filtering methods, as well as determine the most suitable candidates for future optical fiber portal sensors and dosimetry applications. The most sensitive dopant for fiber fabrication was determined by measuring the radioluminescence, thermoluminescence and optically stimulated luminescence (OSL) in response to ionising radiation.

2. Sample Selection and Preparation

Doped silica samples (Table 1) were made using the REPUSIL process (16, 17). In summary, high-purity gas phase formed silica nanoparticles and water-soluble compounds of the doping components (such as AlCl₃ x 6H₂O, rare earth chlorides and ammonium tetra borate) are mixed into an aqueous suspension of very pure silica. After dehydration, purification and vitrification, the processed doped granulates are sintered. The resulting rare earth doped bulk silica rods are homogeneous and near bubble-free. Trace elemental analysis using Intertek Genalysis (www.intertek.com) was performed on

six of the reported samples (Table 1) to compare the glass composition with the nominal fabrication values. Results were converted stoichiometrically to mol%.

For absorbance, photoluminescence and radioluminescence measurements, slides were cut from each sample and polished to 1.2 mm thickness. To improve accuracy for thermoluminescence and OSL measurements, materials were crushed to grain sizes of 125 – 300 μm (18). Approximately 6 mg of these grains were mounted within a 7 mm window on stainless steel discs, held in place by silicone oil spray. The luminescence measurements are all normalised for mass and absorbed dose. Ionising radiation exposures were performed using solid-state foils (Amersham International, UK); beta irradiation used $^{90}\text{Sr}/^{90}\text{Y}$ sources, and ^{241}Am was used for alpha irradiation.

A summary of all experiments is provided in Table 2, indicating detector type, detection range, sample preparation, irradiation dose and integration time.

3. Absorbance

The wavelength dependent transmission of optical fibers is important if they are used as intrinsic sensors. We measured the background absorbance spectra of the polished slides made using the REPUSIL process. Measurements were taken using a Cary 5000 UV-Vis-NIR Spectrophotometer (Agilent Technologies, CA, USA) that made use of nitrogen purging. A Slit Beam Width of 3 nm (± 0.048 nm resolution) with a zero base line correction was used to measure the transmission spectra. Transmission was converted to absorbance and shown in Figure 1. The step-features at 320 and 800 nm, 350 and 850 nm are artefacts caused by the respective grating shifts. Source, detector and gratings were changed from 350 and 800 nm to 320 and 850 nm for the 0.1 Al + 0.005 Tm and 1.5 Al + 0.05 Sm samples to reveal Tm and Sm absorbance features.

Photodarkening was tested using the Ce, La and Tm polished slides. Photodarkening is not the focus of this paper and detailed results will not be shown, however, a reduction in transmission, which we attributed to photodarkening, was seen when radiating samples with a beta source over 23 hours, administering a total dose of 1.38 kGy.

No sharp absorbance features are observed in the reference Al glass because there are no rare earth dopants. Samples with 8 mol% Al content show increased absorbance between 200 and 550 nm when compared to reference samples with lower Al concentrations. The addition of B to the 8 Al sample decreases absorbance below 700 nm (Figure 1).

The La doped sample showed no absorbance peak.

The 0.1 Al + 0.005 Ce sample shows an absorbance peak at 310 nm due to Ce³⁺ consistent with literature (19, 20).

0.1 Al + 0.005 Tm shows sharp peaks at 465 and 790 nm from Tm³⁺ corresponding to transitions from the ¹G₄ and ³H₄ energy levels to the ground state respectively (21).

The Sm doped glass shows peaks at 360 and 400 nm. The 400 nm peak is due to the 4f to 5d transition (22) (⁶H_{5/2} to ⁴F_{5/2} (23)) of Sm³⁺.

The high background absorbance level for both the 1.5 Al + 0.05 Sm and 5 Al + 1.2 La samples is due to increased scattering indicated by the observed mottled appearance in the polished glass samples. This mottled appearance is likely due to a failure to completely sinter the glass during the final step of manufacturing.

The Yb doped samples show a broad peak at 920 nm and a sharp peak at 980 nm from Yb³⁺ corresponding to the transition from ²F_{7/2} excited state to the ground state ²F_{5/2}. Peaks are observed in 1 Al + 0.15 Yb at 260, 330 and 390 nm from Yb²⁺ (24, 25).

The addition of Yb to a sample containing 1 mol% Al increases absorbance, while the addition of B to the Yb and Al sample decreases absorbance. This is consistent with the addition of B to the 8 Al sample showing a reduction in absorbance.

The measured absorbance spectra show the position and strength of rare earth ion absorption transitions in the samples along with the presence of defect centres and other absorbing species such as lower valent Yb²⁺ and Sm²⁺. These absorption results indicate the likely optimal wavelength for excitation photoluminescence and potentially radioluminescence and OSL response.

4. Photoluminescence

Potential emission wavelengths were obtained by measuring the photoluminescence spectra by exciting selected samples with a 7 ns pulsed, 9 mm beam diameter tuneable laser (Opotek Radiant 355 with UV option, OPOTEK Inc, USA) and detection using a Princeton Instruments Acton CCD array (SpectraPro 2300, Roper Scientific, USA) with Lightfield Software (Princeton Instruments, USA). Excitation was provided at 240, 280, 320, 340, 360 and 400 nm with directly scattered light removed using a 355 nm (BLP01-355R-25, Semrock, USA) (for Ce excitation at 240, 280, 320 and 340 nm) or 430 nm long pass filter (FF01-430/LP, Semrock, USA). Depending on the filter, spectra were collected for wavelengths between 360 and 1000 nm using an integration time of 5 s. Spectra are calibrated for wavelength and intensity using a calibration routine within the Lightfield Software and a highly stable LED light source with emission between 400 and 1100 nm (26). The background spectra were also measured and subtracted and results are normalised for excitation pulse power at each excitation wavelength.

The photoluminescence spectra of selected samples are shown in Figure 2.

The Al reference samples shows no photoluminescence response (1 Al shown in Figure 2).

The 0.1 Al + 0.005 Ce sample shows high intensity photoluminescence at 400 nm from the 4f-5d transition (27) when excited with 340 nm.

The 0.1 Al + 0.005 Tm sample shows a small photoluminescence peak at 465 nm from Tm³⁺ corresponding to the transition from the ¹G₄ energy level to ground state during 360 nm excitation.

The same 465 nm band is seen in the absorbance results (Figure 1).

The 1.5 Al + 0.05 Sm sample shows photoluminescence peaks attributed to both Sm²⁺ and Sm³⁺, depending on the excitation wavelength, implying the fabrication process resulted in the reduction of a portion of Sm³⁺ to Sm²⁺. The peaks observed at 570, 610, 650 and 680 nm correspond to Sm³⁺ transitions from ⁶H_{5/2}, ⁶H_{7/2}, ⁶H_{9/2} and ⁶H_{11/2} to ground states, respectively(13, 28). The peaks at 730, 760 and 810 nm correspond to the transitions ⁵D₀ to ⁷F_j (j = 2, 3 and 4 respectively) for Sm²⁺ (Figure 2)(29, 30) and are excited by 280, 360 and 400 nm.

1 Al + 0.15 Yb shows a photoluminescence peak at 980 nm (Figure 2) due to the Yb³⁺ transition from ²F_{5/2} excited state to the ²F_{7/2} ground state in the same wavelength range as for the absorbance results (Figure 1) (31). A broad peak at 530 nm is from the Yb²⁺ electron centre acting as a hole trap which can charge compensate for the aluminium oxygen deficiency centre (24). The same Yb²⁺ peak has been seen when pumping Yb in the UV (32).

5. Radioluminescence

Radioluminescence, also known as scintillation, involves the emission of light during radiation exposure with wavelengths, depending on dopants, ranging from the UV to the infrared. Ionising radiation produces electron-hole pairs and subsequent recombination may occur via a radiative transition, producing luminescence (33).

The Princeton Instruments spectroflurometer (SpectraPro 2300i, Roper Scientific, USA) was used for radioluminescence measurements. These spectra were taken for both alpha and beta irradiation using the foil sources described in Section 2. The radiation sources irradiated one side of the slide and luminescence was collected from the opposite face (Figure 3). Wavelengths in the 400 to 1000 nm

range were measured. No filters were required due to the absence of an excitation light source. Background measurements and cosmic ray events were subtracted and the measured intensity normalised for the activity of the alpha and beta sources. Results for samples that exhibited radioluminescence are shown in Figure 4.

Radioluminescence was seen for samples doped with rare earth ions Ce, Tm, Sm and Yb (Figure 4).

Radioluminescence was not seen in the reference Al and Al + B sample (results not shown).

Radioluminescence of the 0.1 Al + 0.005 Ce shows a broad peak from 300 to 500 nm due to the electric dipole allowed Ce^{3+} 4f to 5d transition (27, 34, 35) from $^2\text{F}_{5/2}$ to $^2\text{D}_{3/2}$ and/or $^2\text{D}_{5/2}$ energy levels (36).

Photoluminescence results (Figure 2) showed a correlating peak at 400 nm excited by 340 nm.

The 1.5 Al + 0.05 Sm radioluminescence results (Figure 4) show a group of six peaks, whereas the photoluminescence results show a group of seven peaks (Figure 2) (summarised in Figure 5). The photoluminescence spectrum shows dominant peaks at 680 and 730 nm, however, the radioluminescence spectrum shows dominant peaks at 610 and 650 nm (Figure 5). 680 and 730 nm peaks are still present in the radioluminescence spectrum, but are smaller than the 610 and 650 nm peaks. The radioluminescence spectrum shows an additional peak at 790 nm due to the $^4\text{G}_{5/2}$ to $^6\text{H}_{13/2}$ transition (28) of Sm^{3+} . Photoluminescence excitation at 240 nm (Figure 2) shows a similar dominant peak wavelength result as the radioluminescence results (Figure 4).

Both the 1 Al + 0.15 Yb and 1 Al + 1 B + 0.25 Yb samples show radioluminescence peaks around 980 nm (Figure 4) consistent with absorbance (Figure 1) and photoluminescence (Figure 2) resulting from the $^2\text{F}_{5/2}$ transition. The Yb sample including B appears to decrease radioluminescence (results not shown).

Higher sensitivity narrower wavelength range radioluminescence measurements were obtained using an Electrontubes 9829B photomultiplier tube (PMT) based detector apparatus with a detection range of 300 to 550 nm. As for previous radioluminescence measurements, excitation was performed with both alpha and beta irradiation on 1.2 mm thick polished glass slides. An ^{241}Am alpha source attenuated to 74 kBq and a $^{90}\text{Sr}/^{90}\text{Y}$ beta source attenuated to 4.14 kBq were used, both integrated

over 100 s. A summary of total counts per kBq for both alpha and beta events over the 300 to 550 nm wavelength range can be seen in Figure 6.

This combination of measurements showed that the rare earth dopants (Sm, Ce and Tm) had higher scintillation than the reference samples (Al and B), confirming that only f-f and f-d transitions of rare earths cause strong radioluminescence. The moderate La response detected using the PMT (Figure 6) could potentially be caused by impurities. Sm and Yb scintillation occurs above 550 nm (Figure 4), hence the intensity is lower with the PMT (300 to 550 nm detection range) for Sm and Yb.

6. Thermoluminescence

Thermoluminescence analysis provides information about the emission wavelength, trap depths, anomalous fading, trapping lifetimes and phosphorescence in luminescent materials (37). Briefly, a population of trapped electrons and holes are formed due to ionising radiation. Heating the irradiated sample stimulates the trapped electrons into the conduction band where the electrons are free to move to recombination centres; each electron-hole recombination then results in an emitted thermoluminescence photon with wavelengths characteristic of the recombination centre. Electrons in energetically deeper traps require higher temperatures in order to be untrapped to the conduction band, hence heating up a sample through a range of temperatures will yield information on these trap depths. Furthermore over time some electrons can potentially tunnel through to adjacent recombination centres in an athermal process and hence recombine electron holes at or below ambient temperatures (37). This mechanism results in a loss of the stored electrons and holes, reducing the measured dose, so is termed anomalous fading. A more detailed description of the thermoluminescence mechanism can be found elsewhere (37, 38).

6.1 Thermoluminescence Glow Curve Measurements

Thermoluminescence was measured using a Riso DA-20 TL/OSL Reader (DTU Nutech, Denmark). All samples were irradiated with a dose of 1 Gy from a $^{90}\text{Sr}/^{90}\text{Y}$ beta source. Samples were measured immediately following irradiation and again after 1 hr to test for anomalous fading and

phosphorescence. Prior to irradiation, samples were pre-heated to remove any signal of formation or dose accumulated from environmental sources. Thermoluminescence measurements were performed between room temperature and 400 °C at a heating rate of 5 °C/s, followed by an additional re-heat to obtain a background, which is then subtracted from the initial thermoluminescence measurement. Luminescence was detected with an EMI 9235 QB PMT filtered with a 7.5 mm thick Hoya U340 filter, which transmits in the 250 to 400 nm region.

Results immediately following irradiation are presented for selected samples (Figures 7 and 8) and are the average of two separate portions of each sample measured under irradiated conditions with a heating rate at 5 °C/s.

Thermoluminescence results show measurable count rates at low temperatures for 0.05 Al (Figure 7) and 0.1 Al + 0.005 Tm (Figure 8) indicating short storage lifetimes with no build-up and the ability to untrap electrons at ambient temperatures. This performance is appropriate for real time monitoring applications with a short duty cycle. The high signal intensities observed at higher temperatures for 8 Al, 1 Al (Figure 7), 5 Al + 1.25 La and 0.1 Al + 0.005 Ce (Figure 8) indicate a highly sensitive dose response by deeper trap populations and suggest suitability of these materials for use as storage phosphors and potentially for dosimetry.

Anomalous fading and phosphorescence results are presented for the 1 Al reference sample and the cerium and thulium doped samples (Figure 9). Measurements are taken in the order the curves are numbered as

- 1) OSL 1 Gy $^{90}\text{Sr}/^{90}\text{Y}$ beta irradiation
- 2) Room temperature phosphorescence
- 3) OSL after 17 minutes
- 4) OSL 1 Gy $^{90}\text{Sr}/^{90}\text{Y}$ beta irradiation
- 5) Initial thermoluminescence (TL) Run 1
- 6) Initial thermoluminescence (TL) Run 2

Phosphorescence and fading after 1 hour

- 7) Thermoluminescence (TL) after 1 hour
- 8) Repeat thermoluminescence (TL) after 1 hour

Where the phosphorescence and fading curve (row 3 of Figure 9) is measured between runs 6) and 7).

Figure 9, row 1 graphs show OSL and phosphorescence. The samples have no sensitivity change with repeated dosing and OSL measurements with curves 1), 3) and 4) overlapping. Curve 2) shows phosphorescence is accounting for less than 1 % of the total signal and fades to negligible, background level counts.

Figure 9, row 2 graphs show thermoluminescence measured promptly following irradiation and after a 1 hr delay following irradiation. Results show the 1 Al reference and Tm doped samples have no anomalous fading indicated by curves 5) and 7) declining with the same slope above 125 °C. The Ce doped sample is hard to interpret due to pre-existing large trapped electron populations giving rise to thermoluminescence peaks above 300 °C overprinting peaks at lower temperatures.

Figure 9, row 3 graphs show phosphorescence and fading over 1 hour. Maximum counts are less than 1 % of the total counts and can be considered within the background response.

6.2 Thermoluminescence Emission Spectra

Thermoluminescence emission spectra were measured using a Fourier-transform thermoluminescence spectrometer (38) to provide spectral information to assist in the interpretation of the thermoluminescence glow curves. Grains were irradiated with a $^{90}\text{Sr}/^{90}\text{Y}$ beta dose of 10 Gy and three dimensional thermoluminescence was performed within 35 mins from the beginning of the radiation application. A heat rate of 5 °C/s from 50 °C to 400 °C was applied to samples and luminescence detected with an EMI 9635 QA PMT. Ramped heating was applied twice to each sample; the second heating acquires a background which is then subtracted. The spectrometer produces an interferogram, which is then analysed using a discrete Fourier-transform and the resultant spectra corrected for spectral response of the PMT (38). Thermoluminescence emission contour plots are shown in Figure 10.

Samples with low radioluminescence response (Figures 4 and 6) also showed low thermoluminescence intensity (Figure 10). 1 Al + 0.15 Yb and 1 Al + 1 B + 0.25 Yb showed a moderate radioluminescence response using a CCD detector detecting between 300 and 1100 nm (Figure 4), which is attributed to Yb^{3+} luminescence at 980nm. No thermoluminescence response was observed for these samples between 250 - 750 nm, since the Yb^{3+} luminescence is outside of the wavelength range of the PMT detector range.

The 1 Al reference sample shows a weak thermoluminescence response between 350 and 550 nm in the thermoluminescence emission spectra (Figure 10) corresponding to a low intensity photoluminescence response (Figure 2). Although the photoluminescence response is in the wavelength range of 500 to 650 nm, the 0.05 Al and 8 Al thermoluminescence response was less than the 1 Al thermoluminescence response (results not shown).

The 5 Al + 1.25 La sample shows a broad low temperature peak of moderate intensity between 300 and 550 nm similar to the thermoluminescence results of the 1 Al reference sample (Figure 9). The addition of La does not seem to have an effect on thermoluminescent intensity, but does shift the

emission band approximately 30 nm towards shorter wavelengths and increases the temperature band.

The broad thermoluminescence peak at 400 nm for 0.1 Al + 0.005 Ce (Figure 10) correlates to a broad photoluminescence (Figure 2) and radioluminescence emission spectra (Figure 4). No clear evidence of anomalous fading was observed (Figure 9).

The thermoluminescence emission spectra of the 0.1 Al + 0.005 Tm sample shows a high intensity Tm peak at 465 nm (Figure 10), corresponding to photoluminescence (Figure 2), radioluminescence (Figure 4) and thermoluminescence curves in Figure 9.

A broad thermoluminescence peak can be seen for 1.5 Al + 0.05 Sm between 600 and 700 nm (Figure 10) corresponding to a similar response seen in photoluminescence (Figure 2) and radioluminescence (Figure 4) results.

In summary the thermoluminescence emission spectra results showed wavelength emissions corresponding to photoluminescence and radioluminescence results and additionally show the temperatures required to untrap electrons, essentially resetting the effect ionising radiation has had on the samples.

7. Optically stimulated luminescence

The mechanism behind Optically Stimulated Luminescence (OSL) is similar to thermoluminescence. However, OSL uses optical stimulation to free electrons rather than the heating used by thermoluminescence. The optical field excites trapped electrons into the conduction band, allowing them to relax back to the ground state via a radiative transition, producing luminescence (39).

OSL emission was measured using a Riso DA-20 TL/OSL Reader (DTU Nutech, Denmark) after 1 Gy of irradiation from a $^{90}\text{Sr}/^{90}\text{Y}$ beta source. OSL was measured in two wavelength regions summarised in Table 2. Measurements taken in the 250 to 400 nm waveband used a Hoya U340 filter and stimulation using a 30 mW, 470 nm diode array that illuminated a 7 mm diameter sample area. Measurements taken in the 320 to 630 nm waveband used a Schott BG39 filter and stimulation at 870 nm, providing 64 mW to the sample area.

OSL was measured over 1021 s at 1 s/channel. The OSL decay curves can be seen in Figure 11. Results for the integrated time taken ($t_{0.05}$) for the signal (I) to decay to 5 % of its maximum value (I_{\max}) for OSL measurements for the 250 to 400 nm waveband and for the 320 to 630 nm waveband are shown in Figure 12. The time taken to reach $t_{0.05}$ was also recorded (Figure 12).

Pulse-anneal and dose response experiments were performed on the 0.1 Al + 0.005 Ce sample. Pulse-anneal experiments show the temperature at which the OSL traps are thermally drained (Figure 13). The pulse-anneal protocol consisted of applying a beta dose, followed by a short illumination pulse at 30 °C, as the initial measurement. This was followed by cycles of heating to incrementally higher temperatures, with each heating followed by a short illumination pulse at 30 °C. The ratio of these pulses to the initial measurements, after depletion correction, reveals the temperature range over which the OSL is thermally eroded (40). Dose response shows the growth in OSL intensity with increasing dose. Here we measured the OSL intensity during the first 20 seconds (background removed) at varying $^{90}\text{Sr}/^{90}\text{Y}$ beta irradiations for repeat runs performed with and without preheat (Figure 14). The 220 °C preheat removed any potentially remaining electrons and electron holes preventing background build-up.

OSL counts give a measured irradiation dose over time. The 0.1 Al + 0.005 Ce sample shows high OSL response at both 470 and 870 nm stimulation with detection ranges of 250 – 400 nm and 320 – 650 nm respectively (Figures 11 and 12) likely because the Ce emission at 400 nm lies within both the CCD and PMT detector ranges. The intense OSL response corresponds to high photoluminescence (Figure 2), radioluminescence (Figure 4) and thermoluminescence (Figure 10) responses at 400 nm. The Ce sample shows increasing intensity with increasing beta irradiance for both preheated and non-preheated runs (Figure 14).

Intense OSL signals are also observed for La and Tm doped samples (Figure 12).

OSL results for the reference Al samples are low (Figure 12), and as with the thermoluminescence results, higher concentrations of Al do not result in increased OSL counts.

The OSL curves show little change in intensity for the 1 Al + 0.15 Yb and 1.5 Al + 0.05 Sm samples (Figure 11B). Times taken during the OSL readout to reach 5 % of the maximum counts are much slower for 870 nm stimulation when compared to 470 nm stimulation (Figure 12). The times taken to reach 5 % of the maximum counts for the 8 Al, 8 Al + 3.4 B, 1 Al + 0.15 Yb, 1 Al + 1 B + 0.25 Yb and 1.5 Al + 0.05 Sm samples (Figure 12) are close to the total experiment time of 1021 s. The lack of intensity change in the OSL curves (Figure 11B) and the times taken to reach 5 % of the maximum counts (Figure 12) imply that 64 mW of power for 1021 s at 870 nm is not enough energy to untrap all the electrons and return them to their ground state in practical timeframes.

8. Discussion

A summary of all results can be seen in Table 3 and Figure 15.

Both scintillation and OSL are mechanisms for detecting radiation response within optical fibres. Scintillation gives a prompt radiation response, whilst OSL accrues dosage over time, acting as a storage phosphor technique. For scintillation applications the rare earth doped silica samples tested give high efficiency scintillation response to the radiation of interest. The samples have a high optical transmission in a detectable waveband. They are immune to sensitivity drift with dose and due to the low radiation doses of interest the samples are not prone to radiation damage. For OSL applications the samples show a high dose sensitivity with large dynamic range in a detectable waveband. The samples also show good signal stability; the OSL and thermoluminescence appear thermally stable, with charge trapping retained over the time span of interest, and they are stable against non-thermal fading processes. Furthermore, the samples showed no sensitivity drift over several heating cycles. These results indicate REPUSIL rare earth doped optical fibers are extremely well suited for detecting ionising radiation using either scintillation or OSL.

The reference Al and B samples along with the La sample did not show a photoluminescence or radioluminescence response. However, luminescent rare earth ion transitions are observed in both

photoluminescence and radioluminescence confirming that the rare earth doping is controlling the luminescence behaviour.

The Al sample showed thermoluminescence peaks at low temperatures (less than 200 °C) indicating the presence of energetically shallow traps in the reference material. These shallow traps have shorter lifetimes and charge may be drained at ambient temperatures, there is therefore less background and build-up of charge from background environmental radiation. Shallow traps are also typically more efficiently stimulated and bleached, in contrast to deeper traps which require longer stimulation to remove an equivalent amount of charge. As such, materials with shallow traps may be more suitable for applications requiring a fast duty cycle and minimal interference from previous dosage events.

The rare earth samples that showed photoluminescence also had strong radioluminescence, thermoluminescence and OSL signatures. Samples with rare earth dopants showed a response from f-f (Sm, Tm and Yb) and f-d (Ce) transitions during photoluminescence, radioluminescence and thermoluminescence and showed a strong response to OSL. The narrow photoluminescence and radioluminescence peaks are consistent with f-f transitions of rare earth ions due to shielding by d orbitals (41).

La did not show any peaks associated with luminescent rare earth transitions in radioluminescence, thermoluminescence or photoluminescence. Measurable counts were seen over a large integration period with a PMT. La showed a moderate response to OSL between 250 and 400 nm, potentially due to impurities.

The absorbance peak of Ce at 310 nm can clearly be identified as Ce³⁺. The combination of Ce and Al forces reducing conditions during fabrication suppressing the formation of Ce⁴⁺ (20). Under oxidising fabrication conditions Ce⁴⁺ results in a peak at 260 nm (20). Ce showed consistently intense luminescence signals in response to each of the measurements because its transition are in the transmission window of the detectors used. The 400 nm broad Ce peak resulting from an f-d transition, was visible during photoluminescence, radioluminescence, thermoluminescence and OSL measurements. Phosphorescence is negligible, with phosphorescence typically less than 1 % of the

total counts, with no samples showing clear evidence of anomalous fading. The Ce OSL counts are three orders of magnitude higher than those seen from fluoride phosphate (4) and two orders of magnitude higher than the terbium doped fluoride phosphate (5) glasses previously measured. The OSL dose response at varying beta irradiations shows that the Ce sample has high dose sensitivity, and demonstrates strong potential for use of this material as a dosimeter. The dose response shows the Ce sample has a dynamic range of approximately eight orders of magnitude; from a detection threshold of 1 μ Gy/mg to saturation at 100 Gy/mg. Higher intensity counts at higher dose measurements for non-preheated samples indicate the presence of remaining trapped electrons and flags the requirement for thermoluminescent “resetting” in future devices to prevent background build up. Pulse-annealing shows that from 25 to 80 °C there is thermal transfer and a portion of electrons and electron holes are retrapping into deep empty traps. Thermal transfer is followed by steady monatomic erosion. Half of the signal is left at 250 °C, but then drops away rapidly as the high temperature peak (seen in the thermoluminescence curves) is depleted. The pulse-annealing shows that some of the OSL response originates from the shallow traps, but most originate from around 300 °C. As the 300 °C traps are depleted the OSL response reduces to near zero. There are no deep significant OSL contributions to the 0.1 Al + 0.005 Ce sample above 400 °C.

Much like Ce, Tm also showed consistently intense luminescence signals in response to each of the measurements. The 465 nm Tm peak from the f-f transition also corresponds to the transmission window of detector ranges used, resulting in high intensity responses to photoluminescence, radioluminescence, thermoluminescence and OSL measurements. Thermoluminescence also showed low temperature peaks for Tm indicating shallow traps, and hence the potential suitability for applications requiring short dose measurement duty cycles.

The Sm sample has a response between 550 - 750 nm. These peaks do not correspond to the detection window of a PMT, but are suitable for silicon detectors with sensitivity in the 300 to 1100 nm region. Interestingly the difference in intensity from photoluminescence and radioluminescence peaks imply Sm²⁺ ions are dominant at 730 nm in the photoluminescence spectrum measured using 400 nm

excitation, whilst Sm³⁺ ions are dominant at 570, 610 and 650 nm in radioluminescence and thermoluminescence spectra measured using an alpha and/or beta source. This indicates that 400 nm light excites predominantly Sm²⁺, which is consistent with Sm²⁺ absorption at 400 nm (42). By contrast, it is likely that the alpha/beta irradiations oxidise the Sm²⁺ ions to Sm³⁺ and thus predominantly only Sm³⁺ luminescence is measured. The thermoluminescence spectrum of the Sm sample shows high intensity peaks above 200 °C implying the existence of deep electron traps. Deep electron traps may enable a build-up of charge from prior dosing that contributes to the total intensity during stimulation of the material and hence constitutes an unwanted drift in sensitivity.

The 1 Al + 0.15 Yb doped sample shows Yb²⁺ absorbance peaks at 260, 330 and 390 nm, whilst with the addition of B (1 Al + 1 B + 0.25 Yb) does not show Yb²⁺ peaks. It is hypothesised that B provides oxidative fabrication conditions preventing the formation of lower valent Yb²⁺. This is consistent with the observation of the lower valent Ce³⁺ and Sm²⁺ ions in the B-free Ce and Sm samples and the absence of Al defect centres. Yb doped samples show an emission peak at 980 nm from the Yb³⁺ ion during photoluminescence, but no thermoluminescence or OSL response. This is due to the 980 nm peak sitting outside of the thermoluminescence and OSL detector ranges of 250 to 750 nm. The presence of Yb in the 1 Al + 0.15 Yb sample relative to the 1 Al reference sample shows increased photoluminescence between 500 and 600 nm. This is possibly due to the Yb²⁺ ions charge compensating the Al based oxygen deficiency centres (24) producing emission at 525 nm. This peak is not observed during radioluminescence or thermoluminescence, potentially due to radiation oxidising Yb²⁺ to (Yb²⁺)⁺, with (Yb²⁺)⁺ showing the same results as Yb³⁺ (43). The radioluminescence spectrum of the 1 Al + 1 B + 0.25 Yb sample does not show a broad peak centred at 525 nm, potentially due to B preventing the formation of Yb²⁺.

The total radioluminescence photon count from rare earth doped samples was approximately 10 times lower for alpha particle events than beta particle events. This result is consistent with previously measured “a-values”; the ratio of alpha/beta efficiency of luminescence production in luminescence

dosimetry (37). The result is due to the extremely high local ionisation density along the alpha particle tracks, saturating the available radioluminescence molecules or luminescence traps.

9. Conclusion

A series of silica samples prepared using the novel rare earth doped reactive powder sintered silica (REPUSIL) technique were tested for their ionising radiation response properties using thermoluminescence, radioluminescence and optically stimulated luminescence. Fabrication using the REPUSIL method allows the production of single material large core robust fibers sensitive to radioluminescence and optically stimulated luminescence. Radioluminescence and optically stimulated luminescence are the mechanisms utilised in fiber optic radiation sensing making the REPUSIL samples well suited for use as portal sensors and in dosimetry applications.

Thermoluminescence, radioluminescence and optically stimulated luminescence were observed if the glass contained luminescent rare earth dopants in the detection wavelength range. Samples doped with Ce and Tm showed intense signals for each of the spectroscopic and radiation-detection measurements applied. Ce showed an increasing response with increasing beta irradiation demonstrating its potential for dosimetry. La showed promising results for radiation-detection measurements, although likely due to impurities, hence La samples with higher purity may not show a response. Yb and Sm doped samples showed emissions at longer wavelengths indicating their suitability for further study using silicon detectors. Reference samples containing Al and B and no rare earth dopants show weak or no response to thermoluminescence, radioluminescence and optically stimulated luminescence confirming that the observed responses to radiation are due to rare earth ion doping.

For optical fiber applications utilising the optically stimulated luminescence method, powder sintered silica materials doped with Ce and Tm appear to be a very promising alternative to the rare earth doped fluoride phosphate glasses previously studied.

10. Acknowledgments

The authors wish to acknowledge funding from the Australian Research Council Research Hub for Australian Copper-Uranium.

The authors wish to acknowledge funding from the Commonwealth of Australia Defence Science and Technology Group.

The authors wish to acknowledge funding from Universities Australia and DAAD as part of the Australia-Germany Joint Research Corporation Scheme.

This work was performed, in part, at the Optofab node of the Australian National Fabrication Facility, a company established under the National Collaborative Research Infrastructure Strategy to provide nano and micro-fabrication facilities for Australia's researchers.

The authors wish to thank Donald Creighton for assistance in operating the Thermoluminescence emission spectrometer.

11. References

1. Huston AL, Justus BL, Falkenstein PL, Miller RW, Ning H, Altemus R. Remote optical fiber dosimetry. *Nuclear Instruments and Methods in Physics Research Section B: Beam Interactions with Materials and Atoms*. 2001;184(1–2):55-67.
2. Huston AL, Justus BL, Johnson JL. Fiber-optic-coupled, laser heated thermoluminescence dosimeter for remote radiation sensing. *Applied Physics Letters*. 1996;68.
3. O'Keeffe S, McCarthy D, Woulfe P, Grattan MWD, Hounsell AR, Sporea D, et al. A review of recent advances in optical fibre sensors for in vivo dosimetry during radiotherapy. *The British Journal of Radiology*. 2015;88(1050):20140702.
4. Kalnins CAG, Ebendorff-Heidepriem H, Spooner NA, Monro TM. Radiation dosimetry using optically stimulated luminescence in fluoride phosphate optical fibres. *Opt Mater Express*. 2012;2(1):62-70.
5. Kalnins CAG, Ebendorff-Heidepriem H, Spooner NA, Monro TM. Enhanced radiation dosimetry of fluoride phosphate glass optical fibres by terbium (III) doping. *Opt Mater Express*. 2016;6(12):3692-703.
6. Antunes P, Domingues F, Granada M, Andre P. Mechanical properties of optical fibres. In: Yasin M, editor. *Selected topics on optical fiber technology*: Intech; 2012.
7. Nguyen LV, Warren-Smith SC, Ebendorff-Heidepriem H, Monro TM. Interferometric high temperature sensor using suspended-core optical fibers. *Opt Express*. 2016;24(8):8967-77.
8. Knight JC. Photonic crystal fibres. *Nature*. 2003;424(6950):847-51.
9. Huston AL, Justus BL, Falkenstein PL, Miller RW, Ning H, Altemus R. Optically stimulated luminescent glass optical fibre dosimeter. *Radiation Protection Dosimetry*. 2002;101:23-6.
10. Benevides LA, Huston AL, Justus BL, Falkenstein P, Brateman LF, Hintenlang DE. Characterization of a fiber-optic-coupled radioluminescent detector for application in the mammography energy range. *Medical Physics*. 2007;34(6Part1):2220-7.

11. Chiodini N, Vedda A, Veronese I. Rare earth doped silica optical fibre sensors for dosimetry in medical and technical applications. *Advances in Optics*. 2014;2014:9.
12. Chiodini N, Vedda A, Fasoli M, Moretti F, Lauria A, Cantone MC, et al., editors. Ce-doped SiO₂ optical fibers for remote radiation sensing and measurement. SPIE 7316, Fiber Optic Sensors and Applications VI; 2009 28 April 2009; Orlando, Florida, United States: SPIE.
13. Chakrabarti K, Mathur VK, Rhodes JF, Abbundi RJ. Stimulated luminescence in rare-earth-doped MgS. *Journal of Applied Physics*. 1988;64(3):1363-6.
14. McKeever SWS. Optically stimulated luminescence dosimetry. *Nuclear Instruments and Methods in Physics Research Section B: Beam Interactions with Materials and Atoms*. 2001;184(1):29-54.
15. Schuster K, Unger S, Aichele C, Lindner F, Grimm S, Litzkendorf D, et al. Material and technology trends in fiber optics. *Advanced Optical Technology*. 2014;3(4):447-68.
16. Langner A, Schötz G, Such M, Kayser T, Reichel V, Grimm S, et al., editors. A new material for high-power laser fibers Proceedings of SPIE; 2008.
17. Leich M, Just F, Langner A, Such M, Schötz G, Eschrich T, et al. Highly efficient Yb-doped silica fibers prepared by powder sinter technology. *Opt Lett*. 2011;36(9):1557-9.
18. Kalnins CAG. Radiation effects in glasses for intrinsic optical fibre radiation dosimetry: University of Adelaide; 2015.
19. Brandily-Anne M-L, Lumeau J, Glebova L, Glebov LB. Specific absorption spectra of cerium in multicomponent silicate glasses. *Journal of Non-Crystalline Solids*. 2010;356(44):2337-43.
20. Unger S, Schwuchow A, Jetschke S, Grimm S, Kirchhof J. Optical properties of cerium-codoped high power laser fibres. Proceedings of SPIE. 2013;8621:862116.
21. Blackburn OA, Tropiano M, Sorensen TJ, Thom J, Beeby A, Bushby LM, et al. Luminescence and upconversion from thulium(III) species in solution. *Physical Chemistry Chemical Physics*. 2012;14:13378 - 84.

22. Li L, Liu, X. Effects of changing the M²⁺ cation on the crystal structure and optical properties of divalent samarium-doped MAI₂Si₂O₈ (M = Ca, Sr, Ba). Royal Society of Chemistry. 2015;5:19734-42.
23. Rare earth doped fiber lasers and amplifiers. Second ed: CRC Press; 2001.
24. Rydberg S, Engholm M. Experimental evidence for the transformation of divalent ytterbium in the photodarkening process of Yb-doped fiber lasers. Opt Express. 2013;21(6).
25. Xia C, Zhao G, Y. H, Zhao X, Hou L. Luminescence of Yb²⁺, Yb³⁺ co-doped silica glass for white light source. Optical Materials 2011;34:769 - 71.
26. Automated wavelength and intensity calibration routines significantly improve accuracy of recorded spectra
27. Lin H, Liang H, Han B, Zhong J, Su Q, Dorenbos P, et al. Luminescence and site occupancy of Ce³⁺ in Ba₂Ca(BO₃)₂. Physical Review B. 2007;76(3):035117.
28. Yamashita N, Asano S. Photoluminescence of Sm³⁺ Ions in MgS, CaS, SrS and BaS Phosphors. Journal of the Physical Society of Japan. 1987;56(1):352-8.
29. Zeng Q, Pei Z, Wang S, Su Q, Lu S. Luminescent Properties of Divalent Samarium-Doped Strontium Hexaborate. Chemistry of Materials. 1999;11(3):605-11.
30. Zeng Q, Kilah N, Riley M, Riesen H. Luminescence Properties of Sm²⁺ -Activated Barium Chloroborates Journal of Luminescence. 2003;104:65-76.
31. Kaczmarek SM, Tsuboi T, Ito M, Boulon G, Leniec G. Optical study of Yb³⁺/Yb²⁺ conversion in CaF₂ crystals. Journal of Physics: Condensed Matter. 2005;17:3771 - 86.
32. Kirchhof J, Unger S, Schwuchow A, Grimm S, Reichel V. Materials for high-power fiber lasers. Journal of Non-Crystalline Solids. 2006;352:2399 - 403.
33. Birks JB. The Theory and Practice of Scintillation Counting. Oxford, United Kingdom: Pergamon Press; 1964.

34. Guillot-Noël O, de Haas JTM, Dorenbos P, van Eijk CWE, Krämer K, Güdel HU. Optical and scintillation properties of cerium-doped LaCl₃, LuBr₃ and LuCl₃. *Journal of Luminescence*. 1999;85(1):21-35.
35. Kramer KW, Dorenbos P, Gudel HU, van Eijk CWE. Development and characterization of highly efficient new cerium doped rare earth halide scintillator materials. *Journal of Materials Chemistry*. 2006;16(27):2773-80.
36. Ebendorff-Heidepriem H, Ehrt D. Formation and UV absorption of cerium, europium and terbium ions in different valencies in glasses. *Optics Materials*. 2000;15:7-25.
37. Aitken MJ. *Thermoluminescence Dating*. London: Academic Press, Inc.; 1985.
38. Prescott JR, Fox PJ, Akber RA, Jensen HE. Thermoluminescence emission spectrometer. *Appl Opt*. 1988;27(16):3496-502.
39. McKeever SWS. *Thermoluminescence of soils*. Davis EA, Ward IM, editors. Cambridge: Cambridge University Press; 1985.
40. Spooner NA, Smith BW, Williams OM, Creighton DF, McCulloch I, Hunter PG, et al. Analysis of luminescence from common salt (NaCl) for application to retrospective dosimetry. *Radiation Measurements*. 2011;46(12):1856-61.
41. Atkins P, Overton T, Rourke J, Weller M, Armstrong F. *The f-block metals*. Shriver & Atkins, Inorganic Chemistry. Fourth Edition ed. Worldwide: Oxford University Press; 2006.
42. Zanatta AR. Coexistence of Sm³⁺ and Sm²⁺ ions in amorphous SiO_x: origin, main light emission lines and excitation - recombination mechanisms. *Optical Society of America*. 2016;6(6).
43. Ebendorff-Heidepriem H, Ehrt D. Effect of Tb³⁺ ions on X-ray-induced defect formation in phosphate containing glasses. *Optical Materials*. 2002;18(4):419-30.

12. Figures

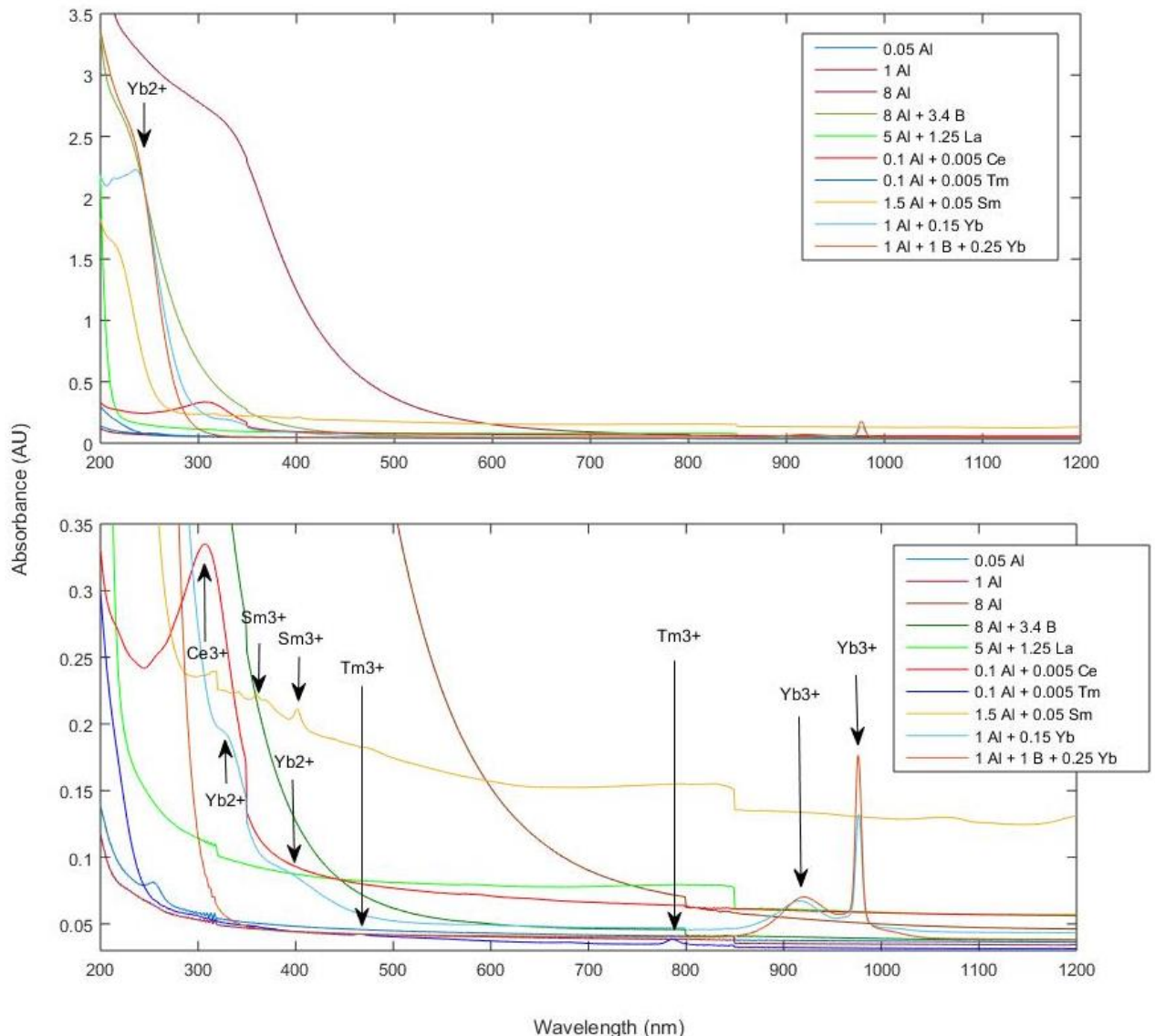


Figure 1: Absorbance measured on 1.2 mm thick polished slides. Labels correspond to transitions that relate to rare earth ions. Note the difference in y-axis scale for the two graphs; the bottom graph is a close up of lower absorbance intensities.

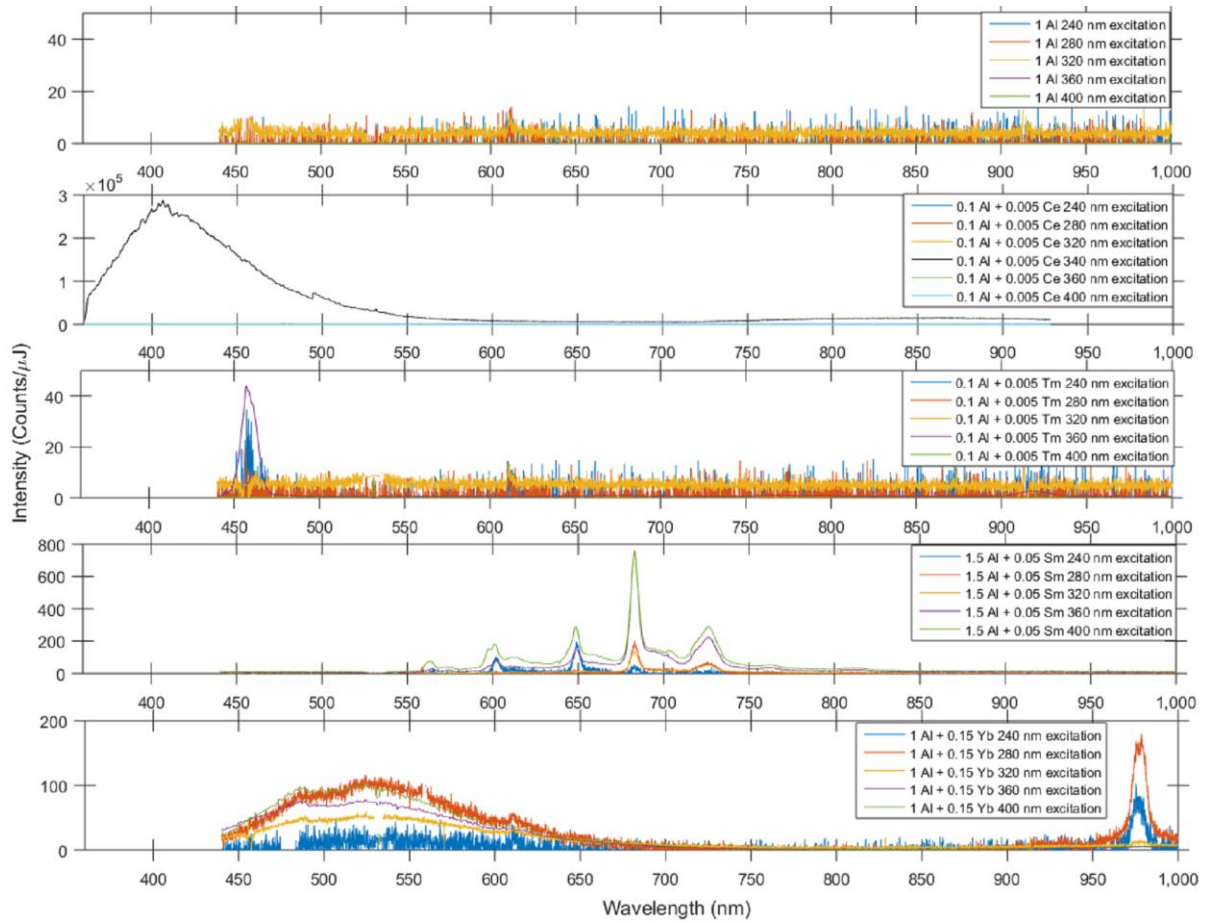


Figure 2: Photoluminescence of selected samples. Note the difference in y-axis scales.

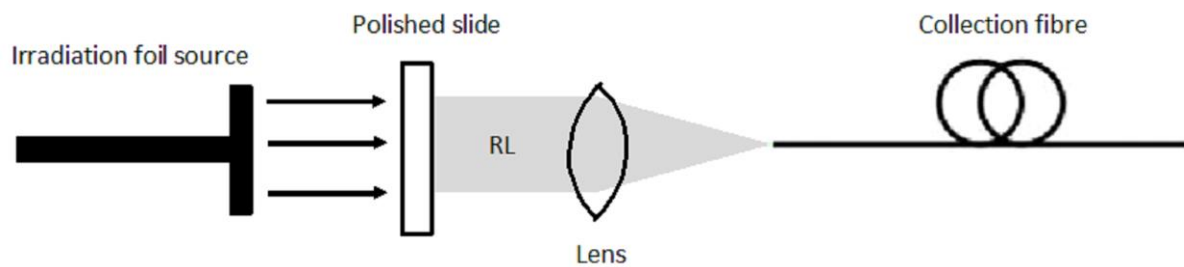


Figure 3: Experimental set up for measuring radioluminescence of polished slides.

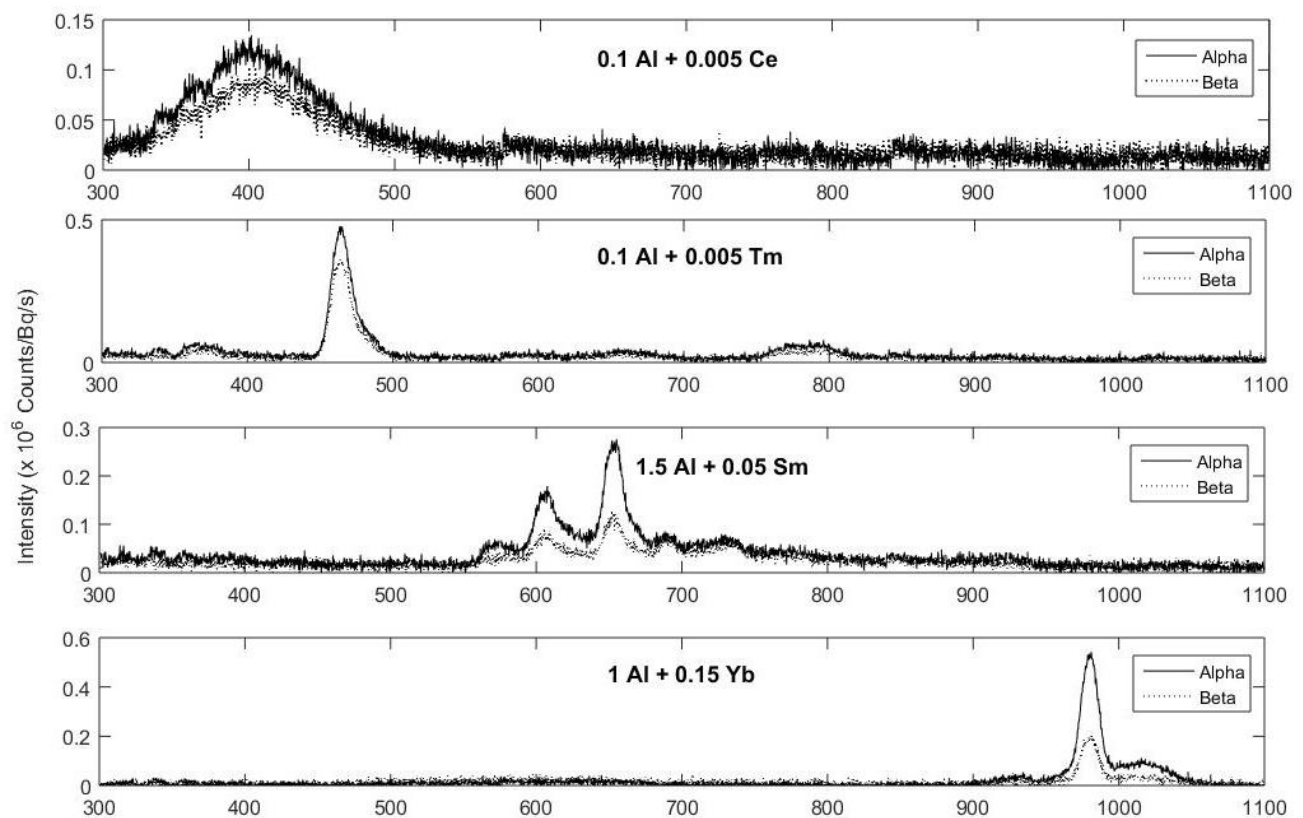


Figure 4: Radioluminescence obtained for alpha exposure using a 14.8 MBq ^{241}Am alpha source and 100 s integration time. Beta exposure used a 185 MBq $^{90}\text{Sr}/^{90}\text{Y}$ beta source with 10 s integration time. Intensity has been normalised to the total absorbed activity per second from the source.

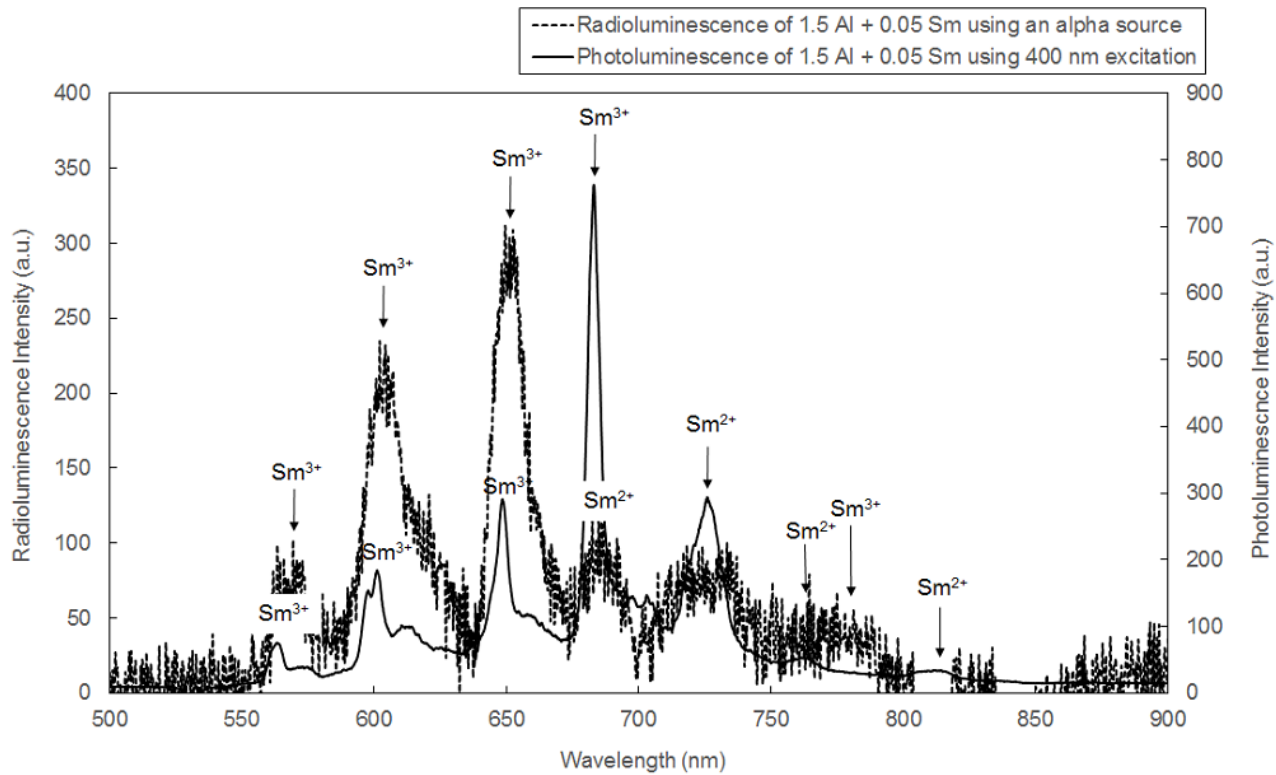


Figure 5: Photoluminescence using excitation at 400 nm and radioluminescence using a 14.8 MBq ^{241}Am alpha source of 1.5 Al + 0.05 Sm. Labels correspond to dominant Sm ions.

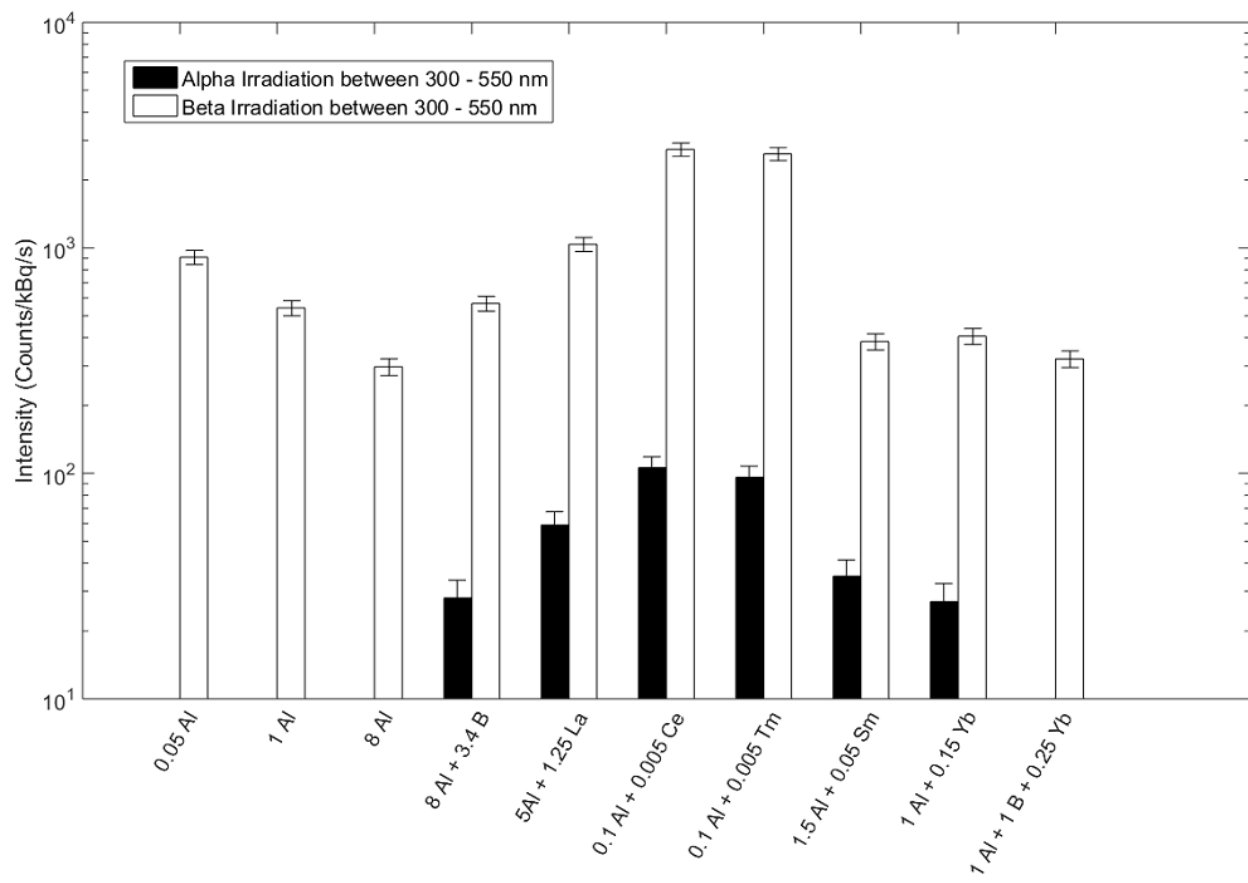


Figure 6: Radioluminescence intensity detected using a PMT between 300 and 550 nm. Excitation with either an ^{241}Am alpha source or a $^{90}\text{Sr}/^{90}\text{Y}$ beta source.

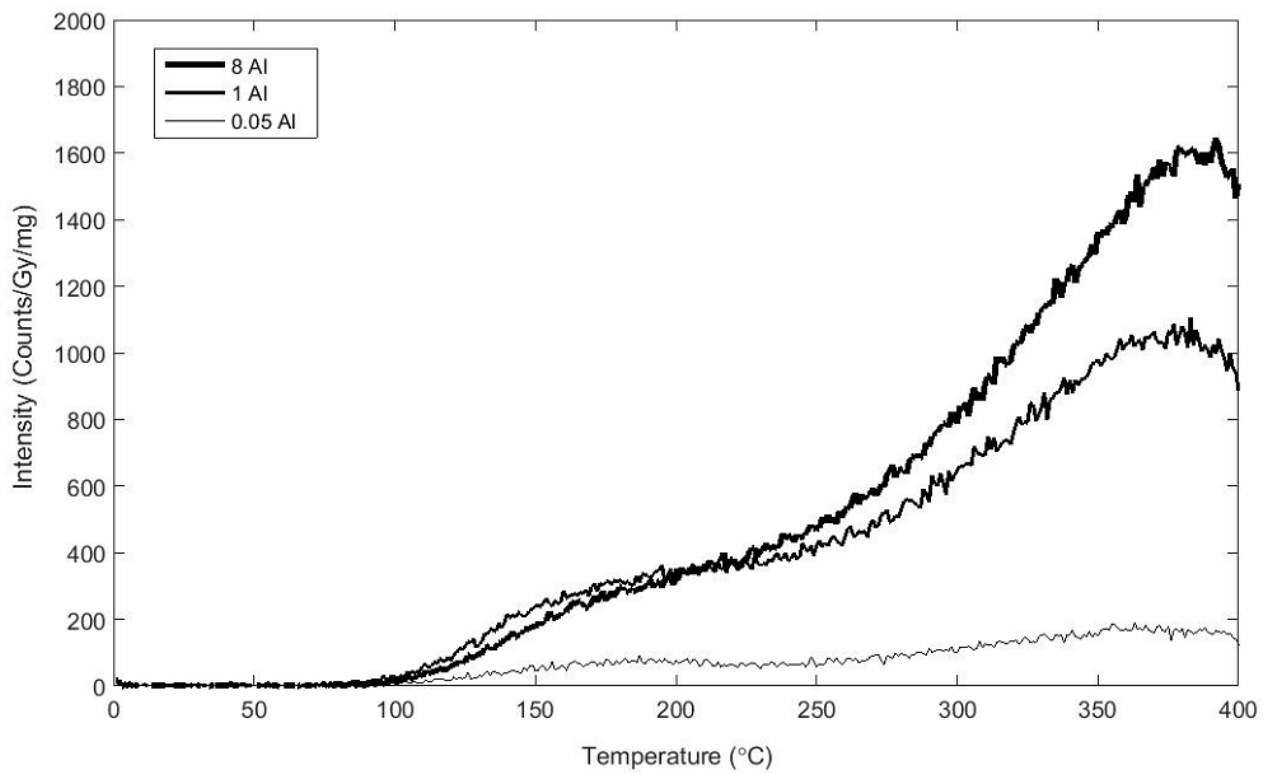


Figure 7: Thermoluminescence curves for the reference Al doped samples; heating rate 5 °C/s, data mass-normalised with reheats subtracted.

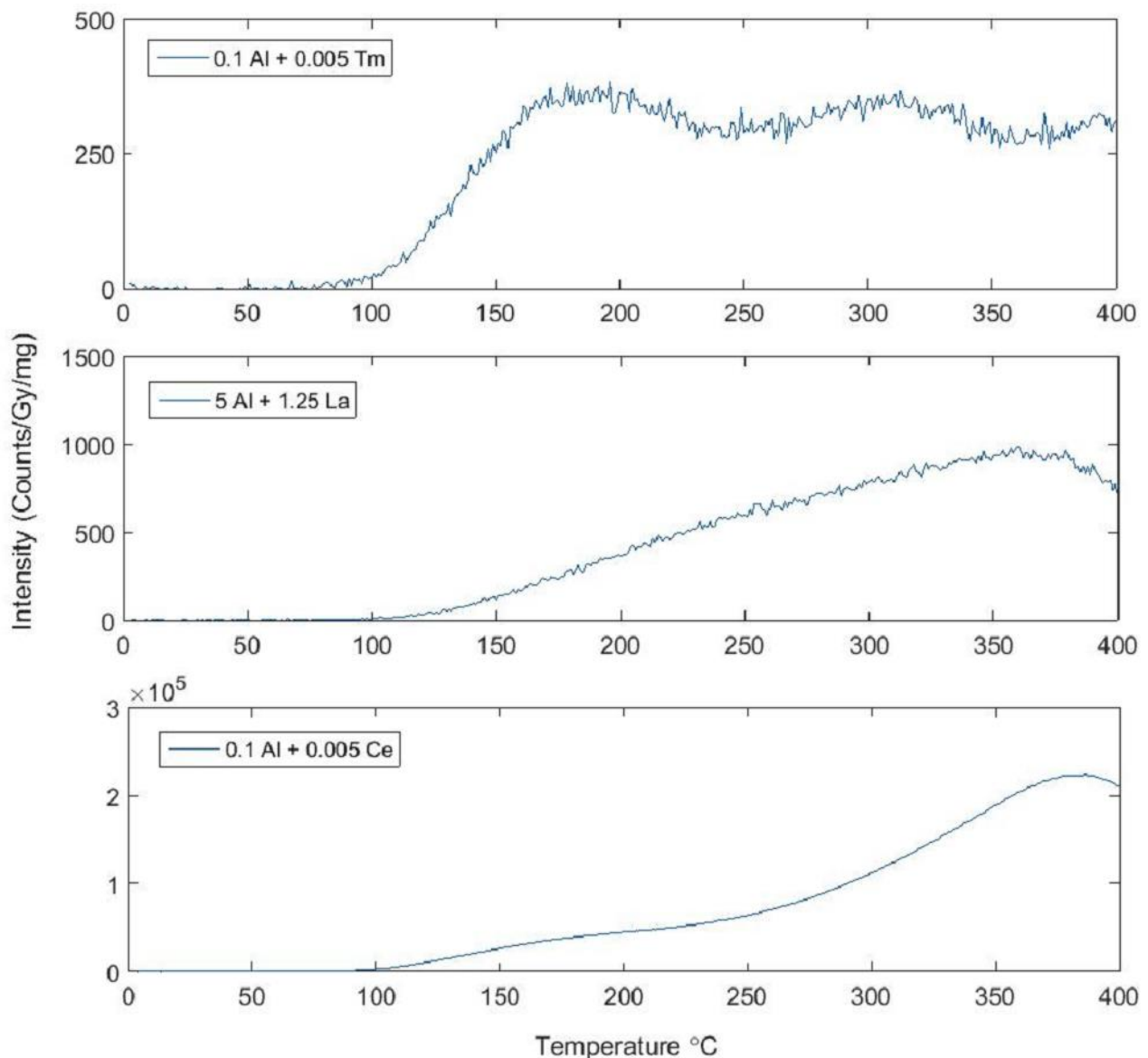


Figure 8: Thermoluminescence curves for selected samples from the rare earth sample series; heating rate 5 $^{\circ}\text{C}/\text{s}$, data mass-normalised with reheats subtracted.

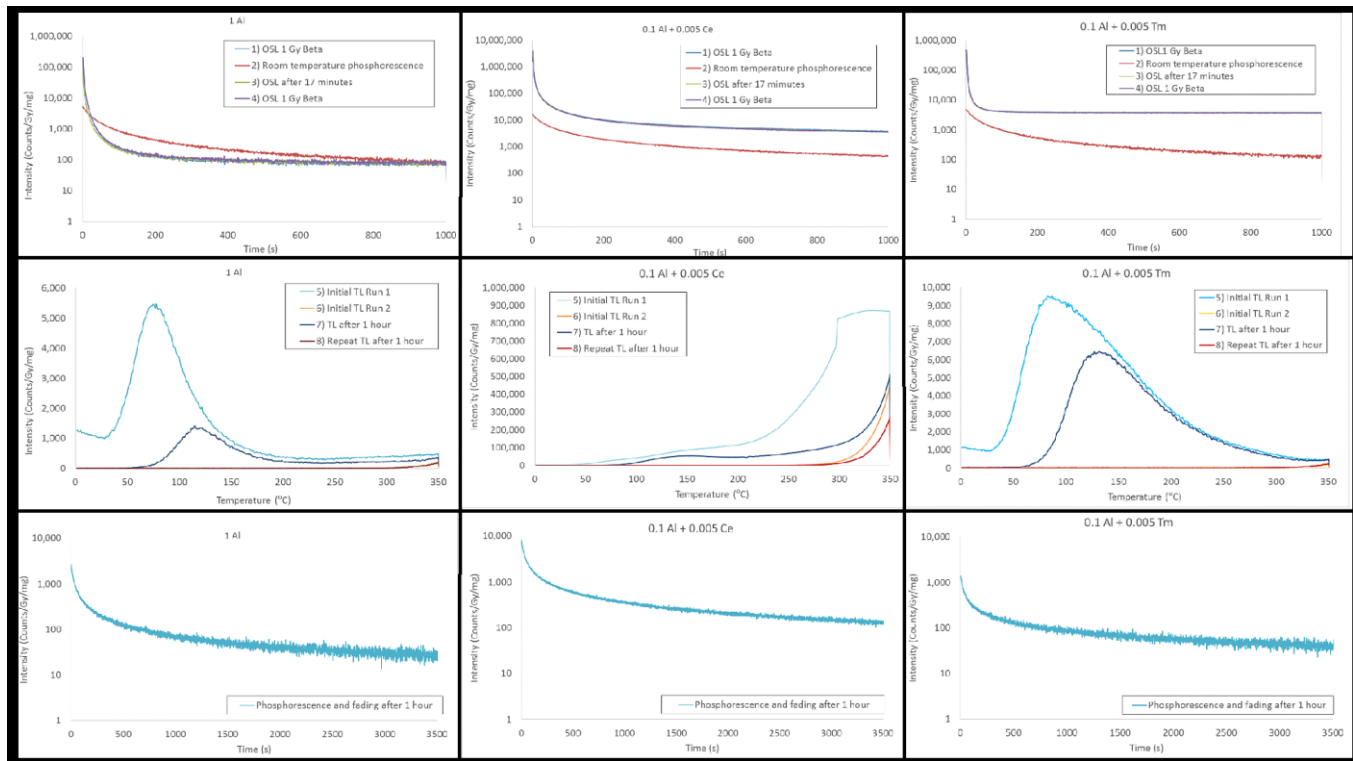


Figure 9: OSL and thermoluminescence (TL) curves showing no clear evidence of anomalous fading and phosphorescence for 1 Al, 0.1 Al + 0.005 Ce and 0.1 Al + 0.005 Tm samples. Note the changes of axis between individual plots.

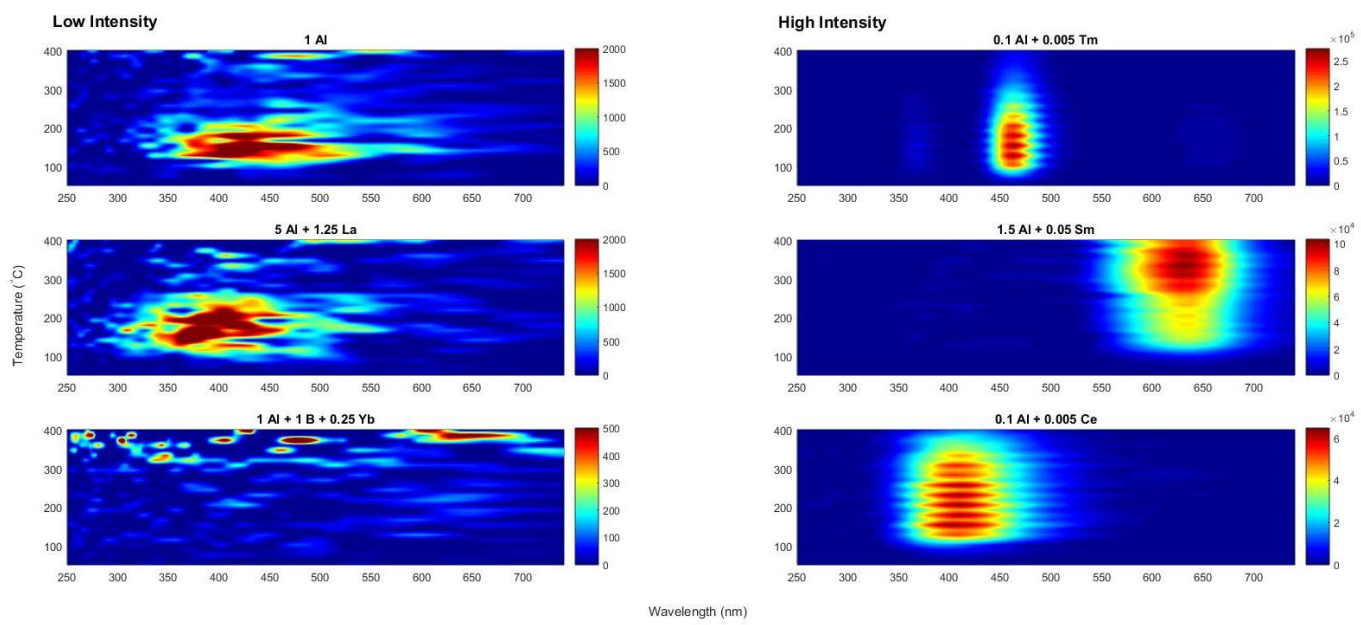


Figure 10: Thermoluminescence emission spectra for selected samples. Note the change in intensity scale between individual plots with low intensity plots on the left and high intensity plots on the right.

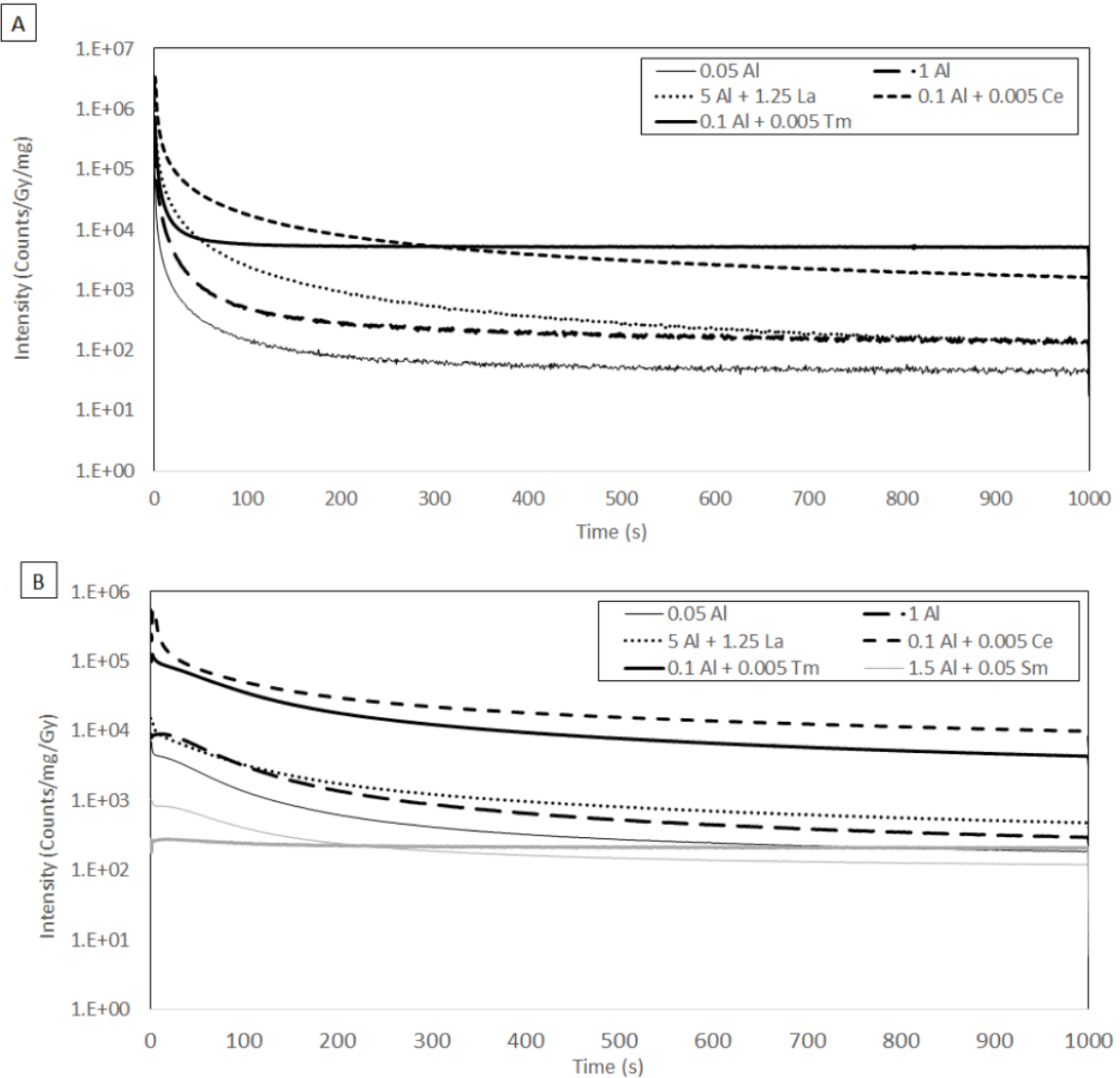


Figure 11: OSL response curves for selected samples measured using A) stimulation at 470 nm and a Hoya U340 filter for detection in the 250 to 400 nm band and B) stimulation at 870 nm and a Schott BG39 filter for detection in the 320 to 630 nm band.

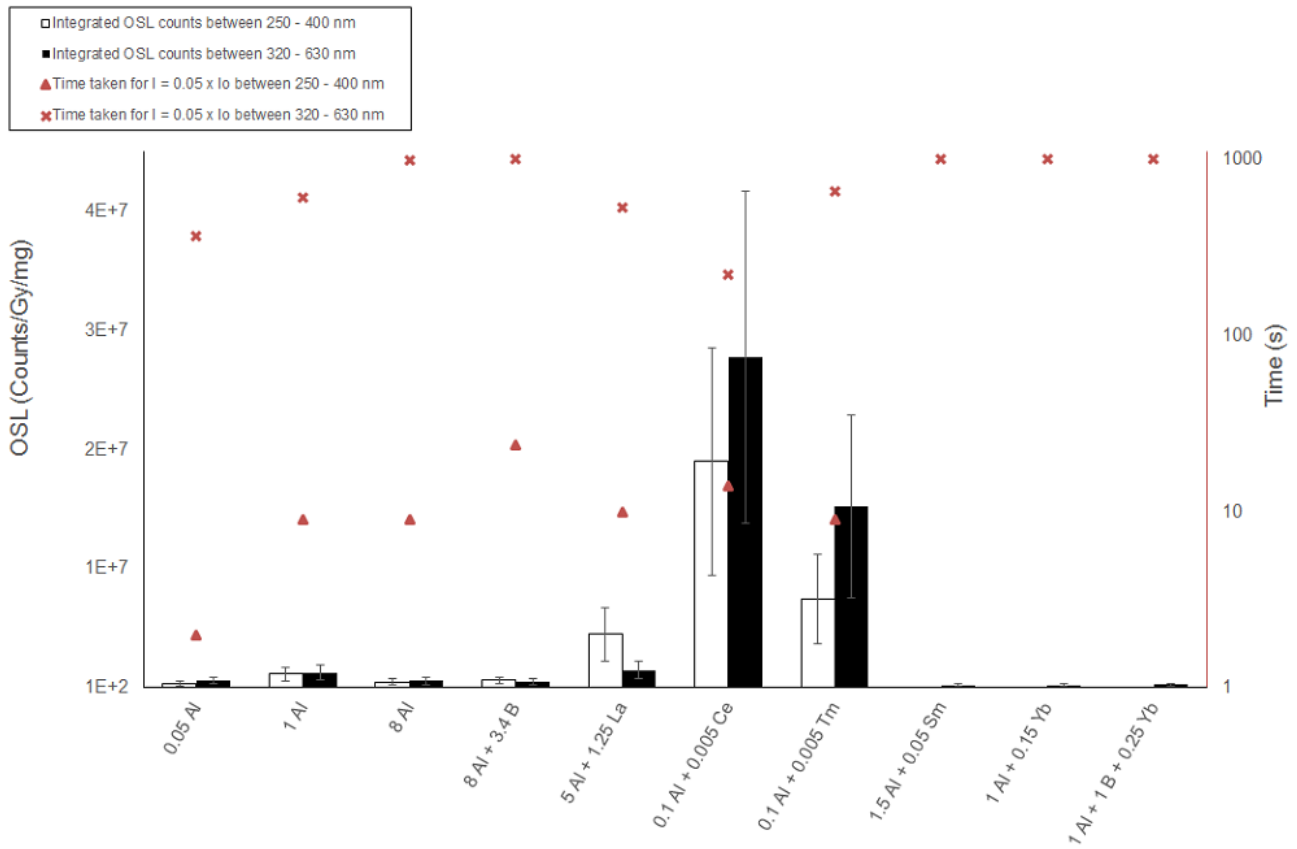


Figure 12: Integrated OSL signal for selected samples measured using stimulation at 470 nm and a Hoya U340 filter for detection in the 250 to 400 nm band (empty bars) and stimulation at 870 nm and a Schott BG39 filter for detection in the 320 to 630 nm band (solid bars). Also shown is the stimulation time required for the OSL to reach 5 % of its maximum value.

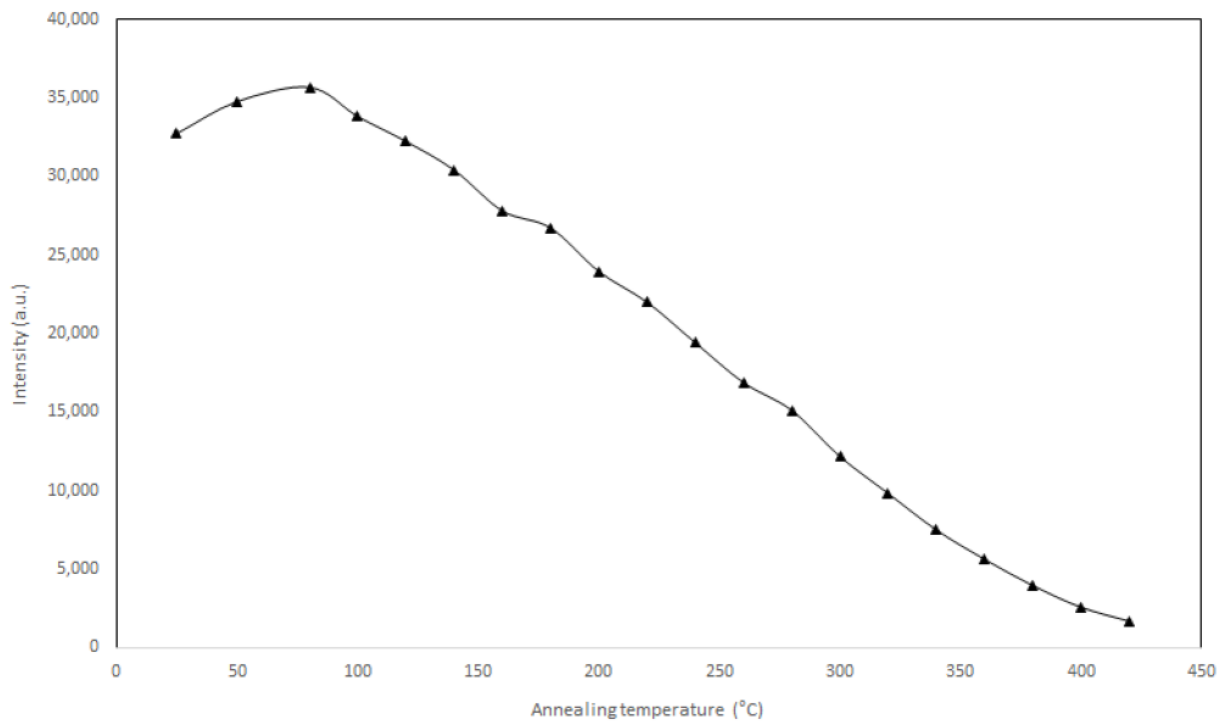


Figure 13: 0.1 Al + 0.005 Ce OSL pulse-anneal response. Data was collected at incremental heating intervals of 20 °C; depletion corrected. Error is incorporated in the symbols and are the counting statistics from the signal integrals and background subtractions.

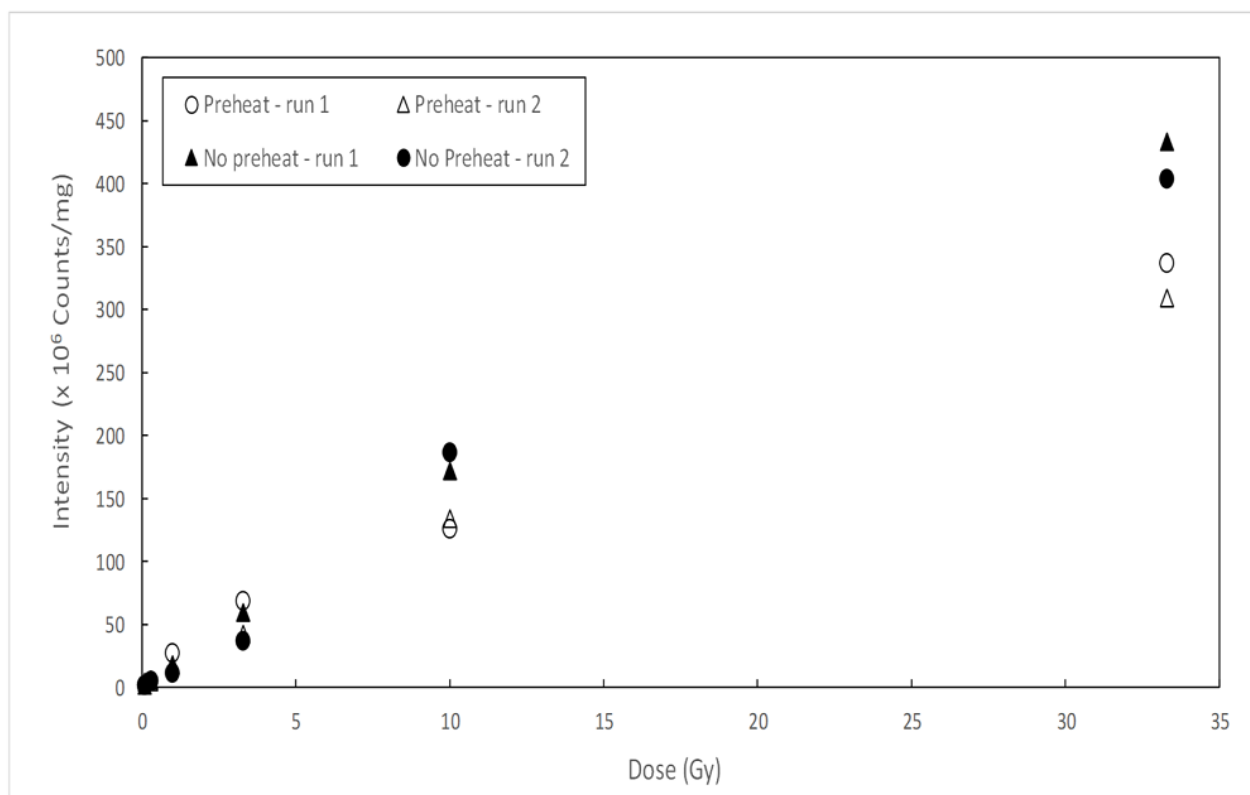


Figure 14: OSL dose response of 0.1 Al + 0.005 Ce at varying beta doses with and without preheat for repeat runs. Error is incorporated in the symbols and are the counting statistics from the signal integrals and background subtractions.

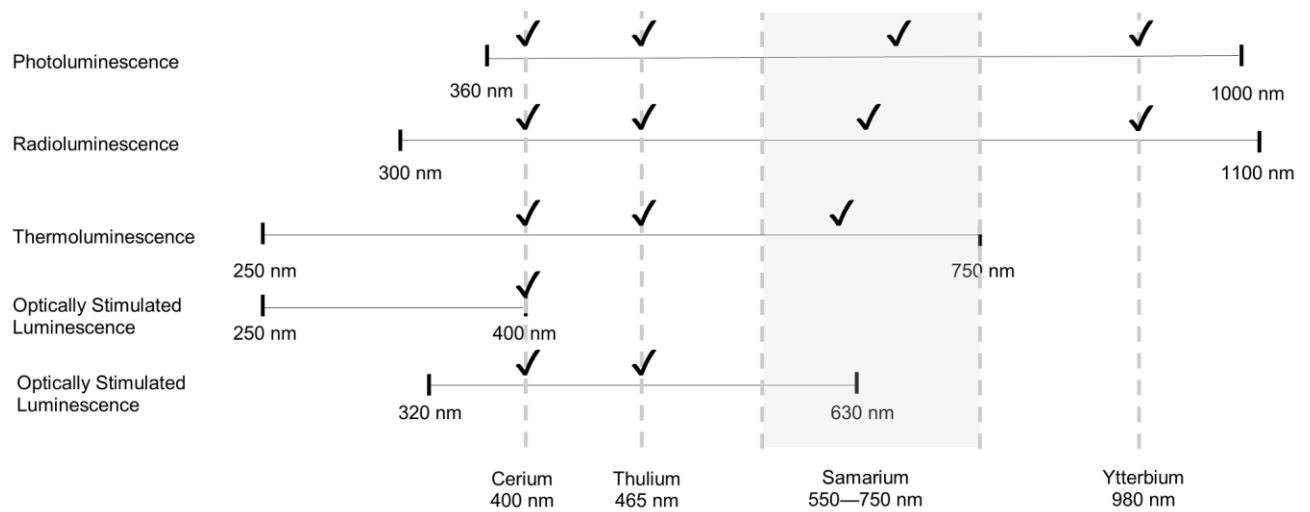


Figure 15: A summary of luminescence measurements, detection wavelengths and peak wavelength results from rare earth dopants in silica. The ticks represent observed results.

13. Tables

Table 1: Composition of REPUSIL samples. Normal font indicates the nominal composition of glasses calculated during fabrication, italic values in parentheses indicate the composition of the samples measured using ICPMS ($\pm 5\%$ error) following fabrication.

	Sample Name	Nominal Composition (mol%) (Measured Composition (mol%))						
		Al ₂ O ₃	B ₂ O ₃	Yb ₂ O ₃	Tm ₂ O ₃	Ce ₂ O ₃	La ₂ O ₃	Sm ₂ O ₃
Reference samples	0.05 Al	0.05						
	1 Al	1.0						
	8 Al	8.0						
	8 Al + 3.4 B	8.0	3.4					
Rare earth doped samples	5 Al + 1.25 La	5.0 (2.11)					1.25 (0.47)	
	0.1 Al + 0.005 Ce	0.1 (0.22)				0.005 (0.005)	(0.001)	
	0.1 Al + 0.005 Tm	0.1 (0.58)			0.005 (0.005)		(0.001)	
	1.5 Al + 0.05 Sm	1.5 (1.28)						0.05 (0.035)
	1 Al + 0.15 Yb	1.0		0.15				
	1 Al + 1 B + 0.25 Yb	1.0 (1.18)	1.0 (1.07)	0.25 (0.25)				

Table 2: Summary of experiment, detector type, spectral band, sample preparation and irradiation dose.

Experiment	Detector type	Detection range	Sample preparation	Irradiation source	Irradiation activity	Integration time
Absorbance	PMT for 300 – 800 nm, PbS for 800 – 1200 nm	300 – 1200 nm	Polished slides	Deuterium lamp for 200 – 350 nm, Xenon lamp for 350 – 1200 nm		90 sec
Photoluminescence	CCD	360 – 1000 nm	Polished slides	240, 280, 320, 340, 360 and 400 nm excitation		5 sec
Radioluminescence	CCD	300 – 1100 nm	Polished slides	$^{90}\text{Sr}/^{90}\text{Y}$ beta	185 MBq	10 sec
				^{241}Am alpha	14.8 MBq	100 sec
Radioluminescence	PMT	300 - 550 nm	Polished slides	$^{90}\text{Sr}/^{90}\text{Y}$ beta	74 MBq	100 sec
				^{241}Am alpha	4.14 MBq	100 sec
Thermoluminescence	PMT	250 – 750 nm	Grains	$^{90}\text{Sr}/^{90}\text{Y}$ beta		10 Gy dose
Optically stimulated luminescence	PMT	250 – 400 nm with a 7.5 mm Hoya U340 filter	Grains	$^{90}\text{Sr}/^{90}\text{Y}$ beta		1 Gy dose
Optically stimulated luminescence	PMT	320 – 630 nm with a 3.0 mm Schott BG39 filter	Grains	$^{90}\text{Sr}/^{90}\text{Y}$ beta		10 Gy dose

Table 3: A summary of peak wavelengths for absorbance and luminescence results for a variety of doped silica samples. Grey cells represent a measured response. Blank cells represent no response.

Observed transition	Absorbance	Photoluminescence	Radioluminescence	Thermoluminescence	OSL	
		Excitation: Various Detection: 360 – 1000 nm	Excitation: alpha and beta Detection: 300 – 1100 nm	Excitation: beta Detection: 250 – 750 nm	Excitation: beta	
		f-f transition (Tm, Sm, Yb) f-d transition (Ce)	f-f transition (Tm, Sm, Yb) f-d transition (Ce)	f-f transition (Tm, Sm, Yb) f-d transition (Ce)	Detection: 250 – 400 nm	Detection: 320 – 630 nm
Sample Name					Stimulation: 470 nm	Stimulation: 870 nm
0.05 Al						
1 Al						
8 Al						
8 Al + 3.4 B						
5 Al + 1.25 La	590 nm					
0.1 Al + 0.005 Ce	310 nm	400 nm	400 nm	400 nm	++	++
0.1 Al + 0.005 Tm	465 nm	465 nm	465 nm	465 nm		++
1.5 Al + 0.05 Sm	400 nm	680 nm	660 nm	630 nm		
1 Al + 0.15 Yb	980 nm	980 nm	980 nm			
1 Al + 1 B + 0.25 Yb	980 nm	Not measured	980 nm			